


# Piezo-Hall effect and fundamental piezo-Hall coefficients of single crystal n-type 3C-SiC(100) with low carrier concentration

Cite as: Appl. Phys. Lett. **110**, 162903 (2017); <https://doi.org/10.1063/1.4980849>

Submitted: 19 December 2016 . Accepted: 04 April 2017 . Published Online: 18 April 2017

Afzaal Qamar , Dzung Viet Dao, Toan Dinh, Alan Iacopi, Glenn Walker, Hoang-Phuong Phan, Leonie Hold, and Sima Dimitrijevic



View Online



Export Citation



CrossMark

## ARTICLES YOU MAY BE INTERESTED IN

[Fundamental piezo-Hall coefficients of single crystal p-type 3C-SiC for arbitrary crystallographic orientation](#)

Applied Physics Letters **109**, 092903 (2016); <https://doi.org/10.1063/1.4962048>

[Piezo-Hall coefficients of n-type silicon](#)

Journal of Applied Physics **64**, 276 (1988); <https://doi.org/10.1063/1.341422>

[Ultra-high strain in epitaxial silicon carbide nanostructures utilizing residual stress amplification](#)

Applied Physics Letters **110**, 141906 (2017); <https://doi.org/10.1063/1.4979834>

Lock-in Amplifiers  
up to 600 MHz



Watch



## Piezo-Hall effect and fundamental piezo-Hall coefficients of single crystal n-type 3C-SiC(100) with low carrier concentration

Afzaal Qamar,<sup>1,a)</sup> Dzung Viet Dao,<sup>1,2</sup> Toan Dinh,<sup>1</sup> Alan Iacopi,<sup>1</sup> Glenn Walker,<sup>1</sup> Hoang-Phuong Phan,<sup>1</sup> Leonie Hold,<sup>1</sup> and Sima Dimitrijević<sup>1,2</sup>

<sup>1</sup>Queensland Micro- and Nanotechnology Centre, Griffith University, Queensland 4111, Australia

<sup>2</sup>School of Engineering, Griffith University, Queensland 4222, Australia

(Received 19 December 2016; accepted 4 April 2017; published online 18 April 2017)

This article reports the results on the piezo-Hall effect in single crystal n-type 3C-SiC(100) having a low carrier concentration. The effect of the crystallographic orientation on the piezo-Hall effect has been investigated by applying stress to the Hall devices fabricated in different crystallographic directions. Single crystal n-type 3C-SiC(100) and 3C-SiC(111) were grown by low pressure chemical vapor deposition at 1250 °C. Fundamental piezo-Hall coefficients were obtained using the piezo-Hall effect measurements as  $P_{11} = (-29 \pm 1.3) \times 10^{-11} \text{ Pa}^{-1}$ ,  $P_{12} = (11.06 \pm 0.5) \times 10^{-11} \text{ Pa}^{-1}$ , and  $P_{44} = (-3.4 \pm 0.7) \times 10^{-11} \text{ Pa}^{-1}$ . It has been observed that the piezo-Hall coefficients of n-type 3C-SiC(100) show a completely different behavior as compared to that of p-type 3C-SiC. Published by AIP Publishing. [<http://dx.doi.org/10.1063/1.4980849>]

Silicon carbide has attracted much attention for electronic applications in a harsh environment due to its large bandgap, high thermal conductivity, and high saturation velocity. A tremendous progress has been made in recent years on material development of SiC, leading to market availability of 4H-SiC and 6H-SiC.<sup>1</sup> Numerous studies on the application of 4H-SiC and 6H-SiC for magnetic field sensing can be found in the literature.<sup>2</sup> However, 4H-SiC and 6H-SiC are much more expensive than 3C-SiC. The capability of hetero-epitaxial growth of SiC on large diameter Si wafers combined with its compatibility with the existing process of micro-electro-mechanical systems (MEMS) makes it a promising choice for magnetic field sensing in harsh environment applications. It can be readily grown over Si substrates of different crystal orientations, e.g., (100), (110), or (111),<sup>3,4</sup> and can reduce the cost significantly. Additionally, the carrier mobility for 3C-SiC is much larger than the carrier mobilities in 4H-SiC and 6H-SiC which makes it an ultimate choice for magnetic field sensing if the interface defects associated with the growth of 3C-SiC over Si are reduced significantly.

Typical growth temperatures for materials are high and the subsequent cooling to room temperature after growth introduces a large amount of stresses in the thin films. These stresses can seriously affect the magnetic field sensitivity of Hall devices. The other factors which can introduce drifts in the magnetic field sensitivity of the Hall devices include a thermal mismatch between the mounting material and chip in die attachment, mechanical impact during device operation, and packaging of the fabricated device.<sup>5-9</sup> Consequently, these various types of stresses introduced into the device can induce drifts in device parameters, offset voltage, temperature behavior, and finally the magnetic field sensitivity.<sup>7</sup> The piezo-Hall effect for Si based Hall devices has been studied for years and a large number of studies on Si can be found in the literature.<sup>10-13</sup> After the measurement of piezo-Hall

coefficients for n-type Si, various studies were conducted to compensate for the stress related sensitivity drifts of Si based Hall devices.<sup>5-13</sup>

The piezo-Hall effect and fundamental piezo-Hall coefficient for single crystal p-type 3C-SiC were reported recently in Refs. 14 and 15. But the study on the piezo-Hall effect in n-type 3C-SiC is still missing. Therefore, this paper aims to investigate the fundamental piezo-Hall coefficients of single crystal n-type 3C-SiC with a low carrier concentration. The effect of the crystallographic orientation on the piezo-Hall effect is also investigated using the Hall devices grown by low pressure chemical vapor deposition (LPCVD) in (100) and (111) crystallographic planes. As low doped n-type 3C-SiC is a preferred material for magnetic field sensors, it is very important to investigate the piezo-Hall effect in this material. The results achieved in this study can be useful for designing n-type 3C-SiC Hall devices for magnetic field sensing.

Single crystal n-type 3C-SiC(100) and 3C-SiC(111) thin films were grown to a thickness of 400 nm on Si(100) and Si(111) substrates by the LPCVD process at the temperature of 1250 °C. Alternating supply epitaxy (ASE) was employed to grow the single crystal 3C-SiC and the precursors SiH<sub>4</sub> and C<sub>3</sub>H<sub>6</sub> were employed as the source of Si and C atoms. The grown films exhibited unintentional n-type conductivity. The full details of the growth process can be found in Refs. 16 and 17. After the growth process, X-ray diffraction (XRD) analysis of the grown films was carried out to confirm the crystal structure followed by the rocking curve to analyze the crystalline quality. Figure 1(a) shows the XRD pattern of the n-type 3C-SiC(100) thin film on Si(100) in the conventional  $\theta$ -2 $\theta$  scan mode. It can be observed from Fig. 1(a) that only the peaks corresponding to the (100) plane are present, which confirms that single crystal 3C-SiC(100) was grown on Si(100). Figure 1(b) shows the rocking curve of the 3C-SiC(100) peak with the observed full width at half maximum (FWHM) value of 0.70°, which shows the good crystalline quality of the grown film. Figures 1(d) and 1(e) show

<sup>a)</sup>Electronic mail: afzaal.qamar@griffithuni.edu.au

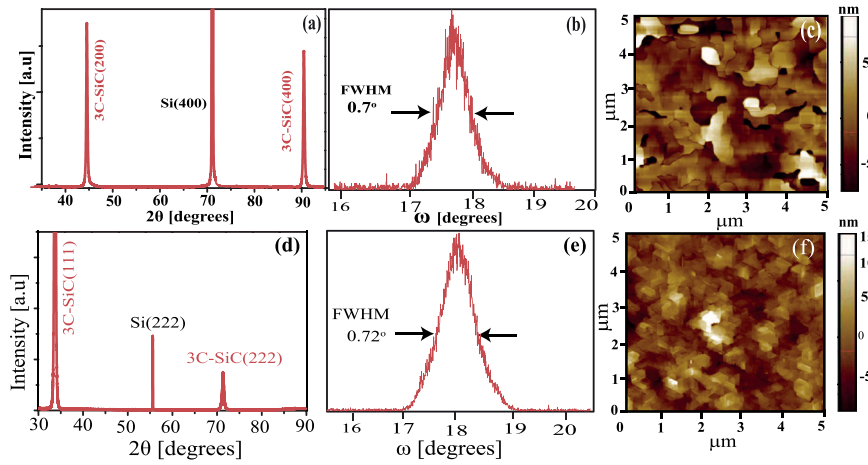


FIG. 1. (a) XRD pattern of single crystal n-type 3C-SiC(100), (b) the rocking curve of 3C-SiC(100), (c) AFM image of n-type 3C-SiC(100), (d) XRD pattern of single crystal n-type 3C-SiC(111), (e) the rocking curve of 3C-SiC(111), and (f) AFM image of n-type 3C-SiC(111).

the XRD pattern and rocking curve of n-type 3C-SiC(111), which confirms that the thin film is single crystal and has good crystalline quality. Atomic force microscopy (AFM) was used to measure the roughness of the grown thin films. The AFM images of n-type 3C-SiC(100) and 3C-SiC(111) thin films for a scan area of  $5\ \mu\text{m} \times 5\ \mu\text{m}$  are shown in Figs. 1(c) and 1(f). The root mean square (RMS) roughness of n-type 3C-SiC(100) was measured to be  $2 \pm 0.5\ \text{nm}$  while that of 3C-SiC(111) was  $1.96 \pm 0.5\ \text{nm}$  which shows the excellent surface morphology of the grown films. The conductance type and carrier concentration of the grown thin film were obtained by hot probe measurements and then confirmed by Hall effect measurements. The carrier concentration of n-type single crystalline 3C-SiC(100) and 3C-SiC(111) was found to be  $5\text{--}8 \times 10^{16}\ \text{cm}^{-3}$ . The carrier concentration of the Si substrates was  $5 \times 10^{14}\ \text{cm}^{-3}$ . The electrical resistivity of n-type 3C-SiC(100) was  $17.4\ \Omega\text{cm}$  with the corresponding hole mobility of  $36\ \text{cm}^2/\text{Vs}$ . The electrical resistivity of n-type 3C-SiC(111) was  $724\ \Omega\text{cm}$  with the corresponding hole mobility of  $0.86\ \text{cm}^2/\text{Vs}$ .

After the growth process, standard photolithography and dry etching processes were used to fabricate the Greek cross shaped Hall devices (Fig. 2(a)). The Greek cross shape was chosen to investigate the stress-induced piezo-Hall effect because it is the standard device shape for Hall measurements. The devices were designed at different angles in the photolithography mask and the direction of dicing of the

beam in particular direction was varied by rotating the mask within the crystal plane. After fabrication of the devices, the wafer was diced into strips with dimensions of  $60\ \text{mm} \times 9\ \text{mm} \times 0.675\ \text{mm}$  to apply stress by the bending beam method. The cantilever method was used to apply the stress to the devices in which one end of the beam with the devices was fixed, while a known force was applied to the other end. Consequently, stresses from 0 to 343 MPa were induced to the n-type 3C-SiC layer to investigate the piezo-Hall effect. The method to numerically calculate the stress-induced into the 3C-SiC layer on the Si strip is reported elsewhere.<sup>18</sup> The second method to apply the stress along the direction of the thickness of the thin film is reported in Ref. 14. The Ohmic contacts were confirmed by the  $I$ - $V$  measurement and horizontal and vertical current leakages from n-type 3C-SiC(100) through to the Si substrate were measured to be less than 2% of the total device current. Therefore, the current leakage is negligible and it does not contribute in the measurements.

In order to evaluate the piezo-Hall effect and calculate the piezo-Hall coefficients, current was applied to the device at terminals 1 and 2, while the change in Hall voltage, corresponding to the change in applied stress, was recorded at terminals 3 and 4 (Fig. 2(a)). In the presence of a constant magnetic field  $B$ , when stress is applied to the device at constant input current, the Hall voltage across terminals 3 and 4 will change with the increase in applied stress, which is called the piezo-Hall effect (Fig. 2(b)). The change in Hall

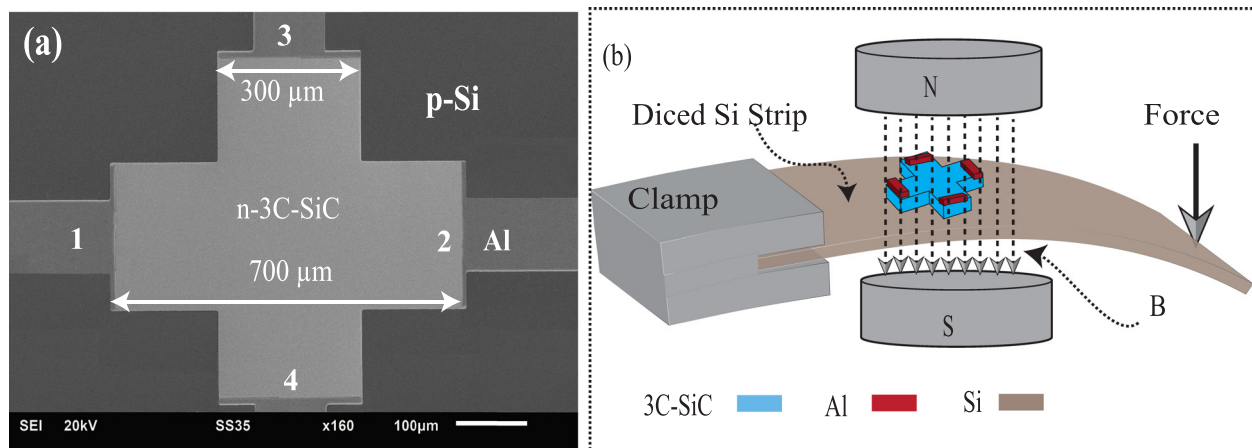


FIG. 2. (a) SEM image of the fabricated Hall device, (b) experimental setup to measure the piezo-Hall coefficients.

voltage was used to calculate the change in the magnetic field sensitivity of the Hall device according to the following relation:

$$\left. \begin{aligned} S &= (V_H/I)/B = R_H(G/t) & [VA^{-1}T^{-1}] \\ \Delta S &= (\Delta V_H/I)/B = \Delta R_H(G/t) & [VA^{-1}T^{-1}] \end{aligned} \right\}, \quad (1)$$

where  $V_H$  is the Hall voltage observed at terminals 3 and 4,  $I$  is the current flowing through terminals 1 and 2 as shown in (Fig. 2(a)),  $B$  is the applied magnetic field,  $R_H$  is the Hall coefficient,  $G$  is the geometrical correction factor, and  $t$  is the thickness of the n-type 3C-SiC thin film. Here,  $\Delta S$  is the change in the magnetic field sensitivity of the Hall devices due to the change in Hall coefficient  $\Delta R_H$  and change in Hall voltage  $\Delta V_H$ . When the stress is applied to the Hall devices, it leads to the change in Hall coefficient  $R_H$  which changes the Hall voltage, ultimately resulting in change in the magnetic field sensitivity of the Hall device. This phenomenon is called the piezo-Hall effect. Here, the change in the magnetic field sensitivity  $\Delta S$  of Hall devices from Eq. (1) will be utilized to study the piezo-Hall effect experimentally. Figure 3(a) shows the change in the sensitivity of the n-type 3C-SiC Hall devices for the (100) plane when the stress was applied along the thickness of the thin film (into the plane), while the magnetic field was applied out of plane. For this particular

configuration, it is difficult to apply the stress along the direction of the thickness of the film and the applied stresses are small in magnitude. Due to the small amount of applied stress, the observed Hall voltage at the constant stress level showed variation, so a linear fitting was used to obtain the required values. The change in magnetic-field sensitivity is negative for this configuration.

Figure 3(b) shows the change in the magnetic field sensitivity of the n-type 3C-SiC Hall devices fabricated in the (100) plane in various directions of current and applied stress. The sensitivity of n-type 3C-SiC Hall devices was measured for three different angles ( $0^\circ$ ,  $45^\circ$ , and  $90^\circ$ ) between the current flow and the longitudinal stress (Fig. 3(d)). The stress was applied in two different crystal orientations ([100] and [110]) (Fig. 3(b)). It can be observed from Fig. 3(b) that the change in magnetic-field sensitivity shows almost linear behavior against the applied stress. It can also be observed from Fig. 3(b) that the change in magnetic-field sensitivity has the equal magnitude in all the six orientations of the device in the (100) crystal plane with the maximum error being  $\pm 5\%$ .

Figure 3(c) shows the change in the magnetic-field sensitivity of the n-type 3C-SiC Hall device in the (111) crystal plane for various directions of applied current and stress. Similar to the (100) plane, the change in the sensitivity of the

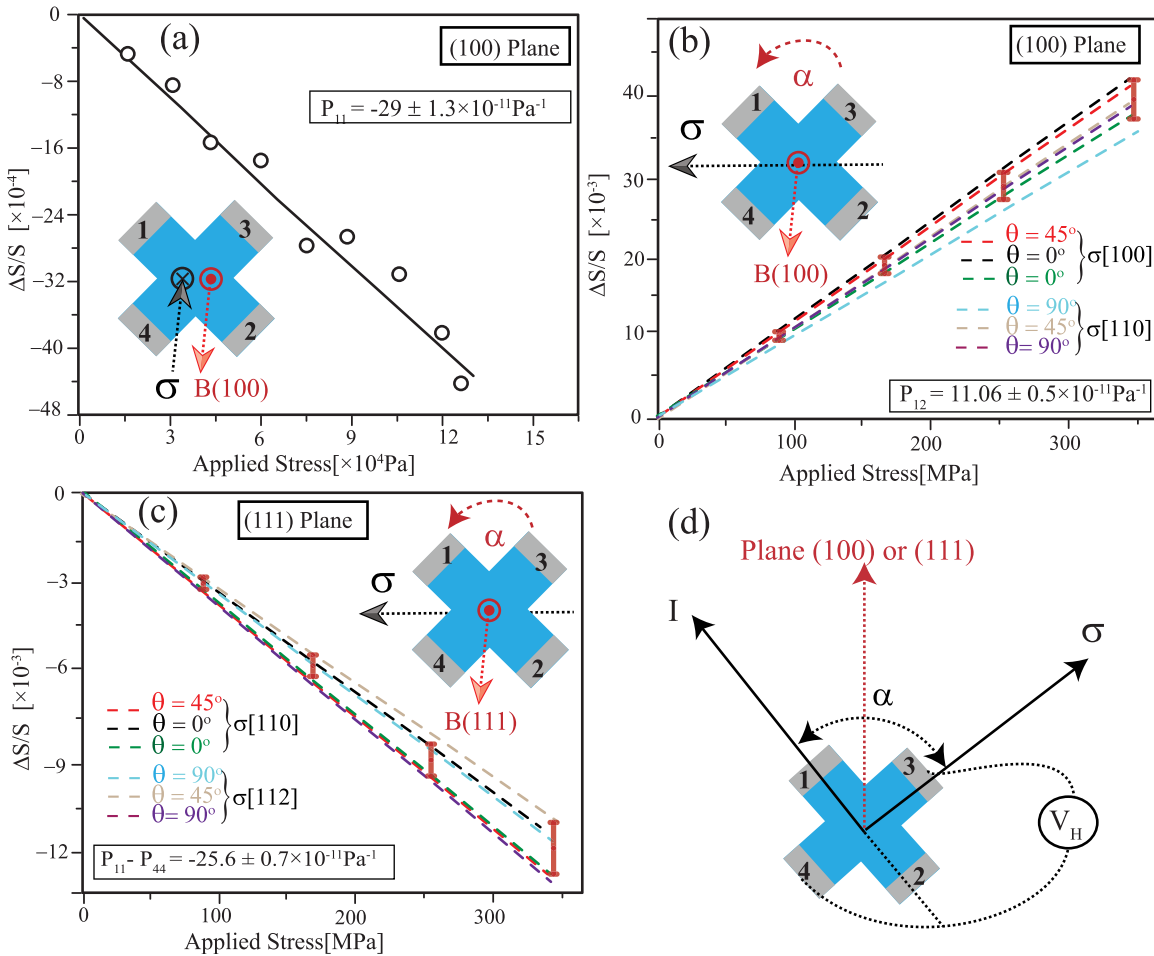


FIG. 3. Effect of applied stress on the magnetic field sensitivity of the fabricated Hall device for various angles of rotation within (100) and (111) planes; (a) Stress along the thickness of the film in the (100) plane, (b) in the (100) plane for different directions of stress and current, (c) for the (111) crystal plane with various angles of rotation, and (d) description of angle  $\alpha$  between the current flow direction and the longitudinal stress  $\sigma$ . The insets show the directions of current, stress, and magnetic field.



n-type 3C-SiC Hall devices was measured for three different angles ( $0^\circ$ ,  $45^\circ$ , and  $90^\circ$ ) between the current flow and the longitudinal stress. The applied stress was in  $[110]$  and  $[1\bar{1}2]$  directions. The change in the sensitivity of the Hall devices in the (111) plane for various directions of current and stress was also positive and is almost equal in magnitude within the maximum error of  $\pm 5\%$ . These results agree with the theoretical analysis of the piezo-Hall effect being independent of the angle of rotation within the crystal plane.<sup>19</sup>

In order to calculate the piezo-Hall coefficients for n-type 3C-SiC(100), the expression for the piezo-Hall effect in terms of piezo-Hall coefficients is required. As the crystal structure of 3C-SiC is similar to that of Si, we use the same expression valid for cubic Si.<sup>19</sup> Hence, the change in the Hall coefficient due to the change in the magnetic field sensitivity of the Hall devices upon application of stress is given by

$$ph = \dot{P}'_{11}\sigma_1 + \dot{P}'_{12}\sigma_2 + \dot{P}'_{13}\sigma_3 + \dot{P}'_{14}\sigma_4 + \dot{P}'_{15}\sigma_5 + \dot{P}'_{16}\sigma_6, \quad (2)$$

where  $\sigma_1$  is the normal stress orthogonal to the wafer,  $\sigma_2$  and  $\sigma_3$  are in plane normal stresses,  $\sigma_4$  is the in plane shear stress which vanishes at a distance of more than chip thickness from the edge of the chip, and  $\sigma_5$  and  $\sigma_6$  are out of plane shear stresses which are normally zero. Note that  $P_{12}=P_{13}$  and  $P_{14}=P_{15}=P_{16}=0$  due to the symmetry relations of the cubic crystal system  $m\bar{3}m$ . Therefore, Eq. (2) reduces to<sup>19</sup>

$$ph = \dot{P}'_{11}\sigma_1 + \dot{P}'_{12}\sigma_2 + \dot{P}'_{13}\sigma_3, \quad (3)$$

where

$$\left. \begin{aligned} \dot{P}'_{11} &= P_{11} - 2P_a \sin^2 \theta (\cos^2 \theta + \sin^2 \theta \sin^2 \phi \cos^2 \phi) \\ \dot{P}'_{12} &= P_{12} + 2P_a \sin^2 \theta \cos^2 \theta (1 - \sin^2 \phi \cos^2 \phi) \\ \dot{P}'_{13} &= P_{12} + 2P_a \sin^2 \theta \sin^2 \phi \cos^2 \phi \end{aligned} \right\}, \quad (4)$$

where  $P_a = P_{11} - P_{12} - P_{44}$  and  $\theta$  and  $\phi$  are the polar and azimuthal angles of the spherical coordinate system.<sup>14</sup> For

n-type 3C-SiC(111),  $\theta = 54.7^\circ$  and  $\phi = 45^\circ$ . In the 3C-SiC(100) plane,  $\theta = \phi = 0^\circ$  when stress is in the  $[100]$  direction and  $\theta = 0^\circ$ ,  $\phi = 45^\circ$  when stress is in the  $[110]$  direction. Incorporating these values in Eq. (3) gives the final influence of stress to the piezo-Hall effect for (100) and (111) planes in 3C-SiC as follows:

$$\left. \begin{aligned} ph_{(111)} &= \frac{\Delta S}{S} = \frac{P_{11} + 2P_{12} - P_{44}}{3} \sigma_1 \\ &\quad + \frac{P_{11} + 2P_{12} - P_{44}}{3} (\sigma_2 + \sigma_3) \\ ph_{(100)} &= \frac{\Delta S}{S} = P_{11}\sigma_1 + P_{12}(\sigma_2 + \sigma_3) \end{aligned} \right\}. \quad (5)$$

For the calculation of piezo-Hall coefficient  $P_{11}$ , the stress was applied along the thickness of the thin film in (100) crystal planes with  $\sigma_2 = \sigma_3 = 0$ . Therefore, from Eq. (5) with stress along the  $[100]$  orientation, the value of  $P_{11}$  is determined to be  $(-29 \pm 1.3) \times 10^{-11} \text{Pa}^{-1}$ , which is completely different from the piezo-Hall coefficient of p-type 3C-SiC(100).<sup>14</sup> For the calculation of piezo-Hall coefficient  $P_{12}$ , uni-axial stress  $\sigma_2$  is applied and we have  $\sigma_1 = \sigma_3 = 0$ . Therefore, the corresponding piezo-Hall coefficient measured using Eq. (5) for n-type 3C-SiC(100) was  $P_{12} = (11.06 \pm 0.5) \times 10^{-11} \text{Pa}^{-1}$ . For n-type 3C-SiC(111) when stress  $\sigma_2$  is applied, again we have  $\sigma_1 = \sigma_3 = 0$ , and the expression  $P_{11} - P_{44} = (-32.4 \pm 0.6) \times 10^{-11} \text{Pa}^{-1}$  can be obtained. Hence, the three independent piezo-Hall coefficients were obtained as  $P_{11} = (-29 \pm 1.3) \times 10^{-11} \text{Pa}^{-1}$ ,  $P_{12} = (11.06 \pm 0.5) \times 10^{-11} \text{Pa}^{-1}$ , and  $P_{44} = (-3.4 \pm 0.7) \times 10^{-11} \text{Pa}^{-1}$ . Using the values of  $P_{11}$ ,  $P_{12}$ , and  $P_{44}$ , the piezo-Hall coefficients for any arbitrary crystal orientation can be determined using Eq. (4).

Figure 4 shows the directional dependence of all piezo-Hall coefficients of n-type 3C-SiC(100) with a low carrier concentration in the arbitrary crystallographic orientation using the spherical plots. The directional dependence is shown in three crystallographic orientations  $\langle 100 \rangle$ ,  $\langle 010 \rangle$ , and  $\langle 001 \rangle$ . The complete description of the spherical coordinate system used and how to obtain the spherical plots is

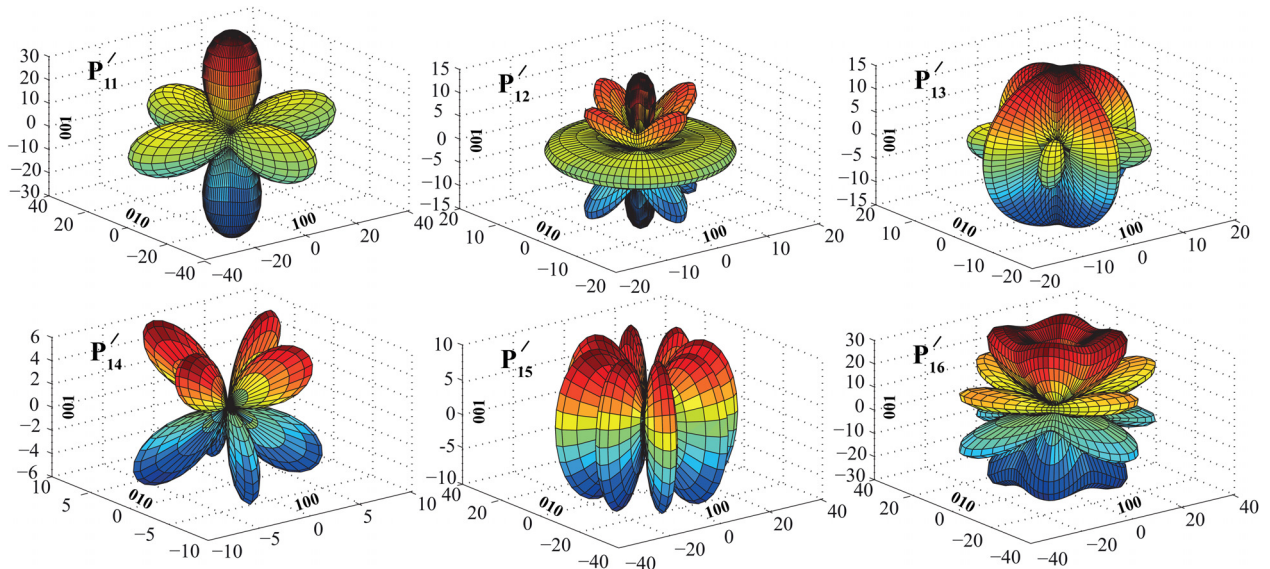


FIG. 4. Spherical plots of piezo-Hall coefficients of single crystal n-type 3C-SiC with a low carrier concentration having the arbitrary crystal orientation in any wafer plane.

TABLE I. Fundamental piezo-Hall coefficients of n-type 3C-SiC and p-type 3C-SiC.<sup>14</sup>

Type of	$P_{11}$	$P_{12}$	$P_{44}$
SiC	$\times 10^{-11} \text{ Pa}^{-1}$	$\times 10^{-11} \text{ Pa}^{-1}$	$\times 10^{-11} \text{ Pa}^{-1}$
<sup>a</sup> n-type	$(-29 \pm 1.3)$	$(11 \pm 0.5)$	$(-3.4 \pm 0.7)$
p-type	$(-2.6 \pm 0.6)$	$(5.3 \pm 0.4)$	$(11.42 \pm 0.6)$

<sup>a</sup>Present study.

given in Refs. 14 and 19. It can be observed from the spherical plots of Fig. 4 that the piezo-Hall coefficients  $\dot{P}_{11}$ ,  $\dot{P}_{12}$ , and  $\dot{P}_{13}$  are maximum for the  $\{100\}$  family of planes and are minimum for the  $\{111\}$  family of planes (Figs. 4(a)–4(c)). The influence of shear stress vanishes for  $\{111\}$ ,  $\{110\}$ , and 100 planes (Figs. 4(d)–4(f)). This behavior of piezo-Hall coefficients is completely different from that of p-type 3C-SiC.<sup>14</sup> Table I shows the fundamental piezo-Hall coefficients on n-type 3C-SiC obtained in this study and the fundamental piezo-Hall coefficients of p-type 3C-SiC, which have been reported elsewhere.<sup>14</sup>

The different behaviour of piezo-Hall effect and different values of the fundamental piezo-Hall coefficients in n-type and p-type 3C-SiC can be attributed to different conduction mechanisms in these semiconductors. For example, in the case of p-type 3C-SiC, the conduction is due to holes distributed in light and heavy hole sub-bands in the valence band. When stress is applied to p-type 3C-SiC, the light hole and heavy hole bands split and hole re-distribution occurs, leading to change in the conductance mechanism and ultimately the Hall coefficient  $R_H$ . In the case of n-type 3C-SiC, the electrons are distributed in 6 equivalent energy valleys. When stress is applied, the electrons repopulate due to energy level shifts, leading to change in electron effective mass and mobility which ultimately results in change of Hall coefficient  $R_H$ . Therefore, the conduction mechanism is completely different in these two semiconductor types, resulting in different behaviours of the piezo-Hall effect. These results have been explained by taking into account the crystal symmetry of 3C-SiC to Si.<sup>20,21</sup> The piezo-Hall effect also depends upon the level of the carrier concentration, but at present, it is difficult to control the carrier concentration as the doping in our thin films is unintentional doping.

In conclusion, the piezo-Hall effect for single crystal n-type 3C-SiC with a low carrier concentration has been investigated for different crystallographic orientations. It has been found that the piezo-Hall coefficients in n-type 3C-SiC with a low carrier concentration show a completely different behavior as compared to p-type 3C-SiC(100) and are much larger in value. The piezo-Hall effect is isotropic in n-type 3C-SiC for (100) and (111) planes. After measurement of

the fundamental piezo-Hall coefficients, the piezo-Hall coefficients for any arbitrary crystallographic orientation can be obtained using the results presented in this study. As single crystal n-type 3C-SiC with a low carrier concentration is a promising candidate for Hall effect devices in the harsh environment, the results of this study can be very useful to understand the stress related magnetic field sensitivity drifts in these devices.

This work was performed in part at the Queensland node of the Australian National Fabrication Facility, a company established under the National Collaborative Research Infrastructure Strategy to provide nano and micro-fabrication facilities for Australia's researchers. This work has been partially supported by the Griffith University's New Researcher Grants. The epitaxial growth was developed as part of Griffiths Joint Development Agreement with SPT Microtechnology, the manufacturer of the Epiflx production reactor.

- <sup>1</sup>J.-L. Robert, S. Contreras, J. Camassel, J. Pernot, E. Neyret, L. D. Cioccio, and T. Billon, *Sens. Actuators, A* **97–98**, 27–32 (2002).
- <sup>2</sup>C. H. Carter, Jr., R. Glass, M. Brady, D. Malta, D. Henshall, S. Muller, V. Tsvetkov, D. Hobgood, and A. Powell, *Mater. Sci. Forum* **353–356**, 3–6 (2001).
- <sup>3</sup>S. Roy, C. Jacob, and S. Basu, *Sens. Actuat. B: Chem.* **94**(3), 298–303 (2003).
- <sup>4</sup>F. La Via, M. Camarda, and A. La Magna, *Appl. Phys. Rev.* **1**, 031301 (2014).
- <sup>5</sup>Y. Liu, Z. L. Rang, A. K. Fung, C. Cai, P. P. Ruden, M. I. Nathan, and H. Shtrikman, *Appl. Phys. Lett.* **79**(27), 4586 (2001).
- <sup>6</sup>A. Nathan and T. Manku, *Appl. Phys. Lett.* **62**, 2947 (1993).
- <sup>7</sup>B. Halg, *J. Appl. Phys.* **64**, 276 (1988).
- <sup>8</sup>R. G. Mani, K. von Klitzing, F. Jost, K. Marx, S. Lindenkreuz, and H. P. Trah, *Appl. Phys. Lett.* **67**, 2223 (1995).
- <sup>9</sup>S. Huber, C. Schott, and O. Paul, *IEEE Sens. J.* **13**(8), 2890 (2013).
- <sup>10</sup>J. M. Cesaretti, W. P. Taylor, G. Monreal, and O. Brand, *IEEE Trans. Magn.* **45**(10), 4482 (2009).
- <sup>11</sup>H. Husstedt, U. Ausserlechner, and M. Kaltenbacher, *IEEE Sens. J.* **11**(11), 2993 (2011).
- <sup>12</sup>R. Steiner, C. Maier, M. Mayer, S. Bellekom, and H. Baltes, *J. Microelectromech. Syst.* **8**(4), 466–472 (2011).
- <sup>13</sup>D. Manic, J. Petr, and R. S. Popovic, *Microelectron. Reliab.* **41**, 767 (2001).
- <sup>14</sup>A. Qamar, D. V. Dao, H.-P. Phan, T. Dinh, and S. Dimitrijević, *Appl. Phys. Lett.* **109**, 092903 (2016).
- <sup>15</sup>A. Qamar, H.-P. Phan, T. Dinh, L. Wang, S. Dimitrijević, and D. V. Dao, *RSC Adv.* **6**, 31191 (2016).
- <sup>16</sup>L. Wang, S. Dimitrijević, J. Han, P. Tanner, A. Iacopi, and L. Hold, *J. Cryst. Growth* **329**(1), 67 (2011).
- <sup>17</sup>L. Wang, A. Iacopi, S. Dimitrijević, G. Walker, A. Fernandes, L. Hold, and J. Chaia, *Thin Solid Films* **564**, 39 (2014).
- <sup>18</sup>H. P. Phan, D. V. Dao, P. Tanner, L. Wang, N. T. Nguyen, Y. Zhu, and S. Dimitrijević, *Appl. Phys. Lett.* **104**(11), 111905 (2014).
- <sup>19</sup>A. Udo, in *Proceedings of IEEE Sensors, 2004*, Vol. 3, pp. 1149–1152.
- <sup>20</sup>J. C. Hensel and G. Feher, *Phys. Rev.* **129**, 1041–1062 (1963).
- <sup>21</sup>D. V. Dao, Ph.D. thesis, Ritsumeikan University, Japan, 2003.